RSC Advances

ROYAL SOCIETY OF CHEMISTRY

www.rsc.org/advances

Table of contents entry

A co-precipitated Mg-Ti nano-composite with high capacity and rapid hydrogen absorption kinetics at room temperature

Yana Liu, Jianxin Zou, Xiaoqin Zeng*, Wenjiang Ding

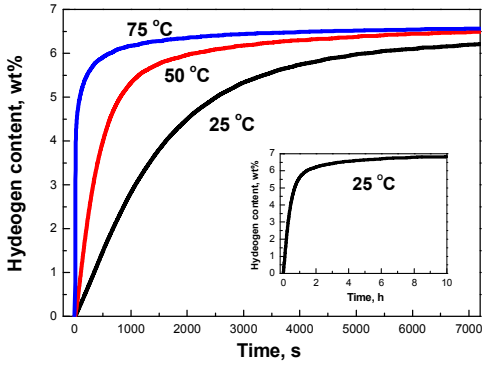

A Mg-Ti nano-composite was co-precipitated through an adapted Rieke method, which exhibits high capacity and superior absorption kinetics at room temperature (~6.2 wt% within 2 h).

A co-precipitated Mg-Ti nano-composite with high capacity and rapid hydrogen absorption kinetics at room temperature

Yanna Liu[a, b], Jinxin Zou[a, b], Xiaoqin Zeng[a, b*], Wenjiang Ding[a,b]

a National Engineering Research Center of Light Alloys Net Forming & State Key Laboratory of Metal Matrix Composite, Shanghai Jiao Tong University, Shanghai, 200240, P. R. China

b Shanghai Engineering Research Center of Mg Materials and Applications & School of Materials Science and Engineering, Shanghai Jiao Tong University, Shanghai, 200240, P.R. China

E-mail address: xqzeng@sjtu.edu.cn.

Abstract

A Mg-Ti nano-composite has been co-precipitated from a tetrahydrofuran (THF) solution containing anhydrous magnesium chloride ($MgCl_2$), titanium tetrachloride ($TiCl_4$) and lithium naphthalide (LiNp) as the reducing agent. X-ray diffraction (XRD), transmission electron microscope (TEM), scanning transmission electron microscope (STEM), and pressure-composition-temperature (PCT) techniques are used to characterize phase components, microstructure and hydrogen sorption properties of the composite. The co-precipitated Mg-Ti nano-composite contains nearly 1.0 wt% of Ti distributed homogeneously on the surface or inside Mg particles having average particle size of about 50 nm. Orthorhombic γ-MgH_2 phase and tetragonal γ-TiH_2 phase are obtained when the Mg-Ti nano-composite is hydrogenated at 75 ^oC. PCT measurements reveal the superior hydrogen absorption property of the Mg-Ti nano-composite: its maximum hydrogen capacity can reach up to 6.2 wt% within 2 h at room temperature under a hydrogen pressure of 3 MPa. The activation energy for hydrogen absorption is determined to be 50.2 kJ/mol H_2. The hydrogenation and dehydrogenation enthalpies of the nano-composite are calculated to be -73.0±1.8 and 75.8±4.7 kJ/mol H_2, close to the standard values for Mg (-74.1± 2.9 kJ/mol H_2). The catalytic effects from the co-precipitated Ti and the tetragonal γ-TiH_2 formed during hydrogenation process lead to the extremely fast absorption kinetics at room temperature.

Keywords: Mg-Ti nano-composite • Rieke method • co-precipitation • hydrogen storage • tetragonal γ-TiH_2 phase

1. Introduction

Mg is considered to be an attractive hydrogen storage material because of its high hydrogen storage capacity (～7.6 wt%), high abundance, non-toxicity, high safety and low cost. However, its poor hydrogen sorption kinetics and unfavorable thermodynamics significantly restrict the practical applications of Mg as the on-board or stationary hydrogen carrier.[1, 2] Several approaches have been adopted to alter its thermodynamics and decrease its kinetic barriers to improve the hydrogen storage properties of Mg, such as (1) alloying Mg with other elements,[3, 4] (2) doping with various catalysts[5-7] and (3) reducing Mg particles to nanoscale.[8-11] Mg-based intermetallic compounds prepared by alloying Mg with other elements show lower dehydriding temperatures as compared to the pure Mg.[3,4] Catalysts, such as transition metals,[5, 12-14] metal oxides,[7, 15-17] halides of tradition metals[6, 18-20] and carbon materials[21-23] have been shown to effectively improve the sorption kinetics of Mg. However, the hydrogen capacity is obviously reduced after catalyst additions compared with the pure Mg.[2, 24] On the other hand, nanoscale Mg exhibits superior sorption properties than that of the coarse grained Mg due to its larger surface area for the nucleation of magnesium hydride and shorter hydrogen diffusion distances for H atoms.[25] Therefore, reducing Mg particles to nanoscale and doping with trace catalysts should be taken into account to obtain a Mg-based composite with high hydrogen capacity and rapid hydrogen sorption kinetics.

Recently, an adapted Rieke method has been introduced to synthesize Mg nano-particles by reducing magnesocene ($MgCp_2$) dissolved in 1, 2-dimethoxyethane

or THF.[9, 11] An air-stable composite (PMMA embedded Mg nanocrystals with an average diameter of 4.9 ± 2.1 nm) enables hydrogen sorption with both high density and rapid kinetics (uptake < 30 min at 200 ^{o}C).[9] Mg nanocrystals with particle size of 25 nm can absorb 95% of its maximum capacity within 60 s at 300 ^{o}C.[11] The adapted Rieke method can provide a simple route for the synthesis of Mg nanocrystals with a desired size. Moreover, doping titanium,[26] titanium hydride,[27, 28] titanium oxide,[18] titanium halides[19, 20] and titanium intermetallics[29] as catalysts into MgH_2/Mg is confirmed to dramatically improve hydrogen storage properties of Mg. MgH_2-0.1TiH_2 composite prepared by ultrahigh-enery-high-pressure milling (UEHP) can absorb 4 wt% of hydrogen in 4 h at room temperature under 2 MPa hydrogen pressure.[28] The hydrogen absorption kinetics of nanocrystalline Ti-catalyzed MgH_2 prepared by a homogeneously catalyzed synthesis method is 40 times faster than commercial MgH_2 at 300 ^{o}C.[30] The dehydriding properties of the ball milled MgH_2 can be remarkably enhanced through coating multi-valence Ti-based nano-catalysts with the onset dehydriding temperature of about 175 ^{o}C.[31] In the present work, a Mg-Ti nano-composite was co-precipitated through the adapted Rieke method. The hydrogen sorption kinetics of the Mg-Ti nano-composite was investigated and the mechanism of catalytic effects from Ti was also proposed.

2. Experimental details

2.1 Sample preparation

In this work, an anhydrous magnesium chloride ($MgCl_2$) was used as the Mg ion source instead of $MgCp_2$. The Mg-Ti nano-composite was co-precipitated from a

homogeneous THF solution including anhydrous $MgCl_2$, titanium tetrachloride ($TiCl_4$) and lithium naphthalide (LiNp) as the reducing agent. It is known that $TiCl_4$ can be reduced to Ti (0) by another metal or metallic hydride reagent such as Li, Mg, Zn, or $LiAlH_4$.[32-34] During the sample preparation process, naphthalene is used as electron carrier to speed up the reaction due to the high melting point of Li.[35] Therefore, the co-precipitation process of the Mg-Ti nano-composite may follow reactions as:

$$MgCl_2 + 2Li \rightarrow Mg(0) + 2LiCl \qquad (1)$$

$$TiCl_4 + 4Li \rightarrow Ti(0) + 4LiCl \qquad (2)$$

These reactions were performed in an argon glove-box to avoid the influence of oxygen and moisture. Both the oxygen and water vapor levels inside the glove-box were kept below 1 ppm. Anhydrous $MgCl_2$ (99.9%), naphthalene (AR), Li (99.9%) and $TiCl_4$ (99.99%) were purchased from Aladdin Reagent Database. In raw materials, Ti: Mg was kept in a weight ratio of 1: 9. LiNp/THF solution (blackish green) was prepared by stirring vigorously the mixture of naphthalene (14.96 g) and lithium (0.81g) in the freshly distilled THF at room temperature. Anhydrous $MgCl_2$ (4.7605g) was dissolved in the freshly distilled THF (400 mL) while stirring vigorously at 60~70 °C to form a transparent solution, and then the solution was cooled down to room temperature. $TiCl_4$ (0.31 mL) was also dissolved in the freshly distilled THF (50 ml) and stirred to form a yellow solution at room temperature. $TiCl_4$/THF was mixed with $MgCl_2$/THF, and the solution was dropped into LiNp/THF while stirring vigorously for 24 h at room temperature. At last, the resultant product was isolated by centrifugation, washed with freshly distilled THF three times, and dried by vacuum

pumping to remove the residual THF. The sample was placed vacuum for 12 h at room temperature. The vacuum level is about 1.33×10^{-2} Pa.

2.2 Characterization

Phase identifications of as-prepared samples were performed by X-ray diffraction（XRD）using an apparatus (D/max 2550VL/PCX) equipped with a Cu K_α radiation source. In order to isolate the sample from air, the sample powder was put on a designed XRD holder and sealed with scotch tape in the glove-box. The morphology and microstructure of as-prepared samples were observed by using a JEM-2100F transmission electron microscopy. The Ti loading in the Mg-Ti nano-composite was analyzed by energy dispersive spectrometer (EDS). As the co-precipitated Mg-Ti nano-composite is extremely active, the activation process is not necessary for all samples before measurements of hydrogen storage properties. The hydrogen sorption behaviors of as-prepared samples were examined using a Sievert apparatus (Type PCT-2, Shanghai Institute of Microsystem and Information Technology). For auto pressure-composition-temperature (P-C-T) measurement, 0.4 g of the sample was loaded in a custom-made autoclave with a hydrogen pressure maximum limit of 4 MPa and operating temperatures of 250, 275, 300, 325, 350 and 375 °C, respectively. Hydrogen absorption kinetic measurements were done at 25, 50 and 75 ^{o}C under 3 MPa hydrogen pressure for 10 h, respectively. A dwelling time of 1 h is set between two PCT measurements. Desorption performance of hydrogenated nano-composites was examined using diffraction scanning calorimetry (DSC, Netzsch STA 449F3) at heating rates of 3, 5 and 10 ^{o}C/min under Ar gas flow.

3. Results and discussions

3.1 Microstructure characterization of the Mg-Ti nano-composite

Figure 1a and 1b presents the XRD patterns of as prepared Mg-Ti nano-composite and the nano-composite hydrogenated at 75 ^{o}C for 2 h, respectively. As can be seen in Figure 1a, almost all broad diffraction peaks of the Mg-Ti nano-composite can be indexed with the hexagonal Mg phase along with a weak peak from MgO, while the characteristic peak of Ti is absent. Formation of MgO phase is due to possible oxidation that occurred during sample preparation for the XRD analysis. The absence of Ti peaks is likely due to the fact that Ti synthetized from solution is in the form of extremely fine particles or amorphous. Alternatively, the amount of Ti in the Mg-Ti nano-composite is too low to generate detectable diffraction intensity. The average crystallite size of Mg in the Mg-Ti nano-composite is calculated to be 23.1 nm using Scherrer's equation.[36] From Figure 1b, it is observed that the majority phase of the hydrogenated Mg-Ti nano-composite is tetragonal β-MgH_2, with a small amount of orthogonal γ-MgH_2, tetragonal γ-TiH_2, Mg and MgO. Residual Mg means that some large Mg particles have not been fully hydrogenated under the given conditions. The metastable γ-MgH_2 has been observed after ball milling of β-MgH_2[8] and the hydrogenation of Mg/Pd thin films prepared using magnetron sputtering method.[37, 38] Previous investigations have shown that the deformations and structural defects formed during the ball milling or the hydrogenation process contribute to the phase transformation from β-MgH_2 to γ-MgH_2.[37, 38] Norberg et al.[11] have hypothesized that the density of defect sites formed

through the adapted Rieke method increases with reducing the particle size. In this work, it is possible that high density of defects formed in the Mg lattice during the preparation process due to the addition of $Ti/TiCl_4$. The high density defects still remain in the nano-composite after hydrogenation at 75 ^oC, leading to the formation of γ-MgH_2 phase. The appearance of tetragonal γ-TiH_2 shows that Ti can be hydrogenated at 75 ^oC. As can be seen in Figure 1c, When the Mg-Ti nano-composite absorbs hydrogen at 75 ^oC again after dehydrogenation at 300 ^oC, γ-MgH_2 phase is absent due to the removal of the lattice distortion and structural defects in Mg nano particles at high temperatures. Similar phenomenon has also been observed in the ball milled pure MgH_2 and in Mg/Pd thin films[37, 38], which is attributed to the fact that γ-MgH_2 is less thermodynamically stable than β-MgH_2. The tetragonal γ-TiH_2 phase with the lattice parameters a=0.312 nm and c=0.418 nm and the strongest diffraction peak located in the 2θ of 40.87 ^{o} has been reported previously.[39-42] Such structure is not the same as the tetragonal ε-TiH_2 phase prepared by reactive ball milling with the strongest diffraction peak located in the 2θ range of 34~36 ^{o}.[27] Tetragonal γ-TiH_2 was formed within titanium matrices during cathodic pretreatments carried out at room temperature.[39-42]

Scanning transmission electron microscope (STEM) micrograph and the selected area electron diffraction (SAED) pattern of the Mg-Ti nano-composite are shown in Figure 2a and 2b, respectively. The Mg-Ti nano-composite is composed of irregular shaped particles aggregating together with their particle sizes ranging from 40 to 60 nm. The average particle size is determined to be about 50 nm. Compared with the

average crystallite size of Mg calculated from XRD results (23.1 nm), some larger particles observed in TEM are possibly made-up of multiple crystal domains. In contrast, Mg nanocrystals prepared through the adapted Rieke method by Norberg et al. have their particle size of about 25 nm.[11] It suggests that the addition of $Ti/TiCl_4$ has little effect on reducing the particle size of Mg nanoparticles. This result is accordance with the research of Nelson,[43] who points out that Mg grains are easily coarsened by the presence of Ti even at very low concentration. In the corresponding SAED pattern shown in Figure 2b, the diffraction rings or points can be indexed with Mg and MgO phase. This is in accordance with XRD result. Formation of MgO phase is due to the possible oxidation that occurred during the preparation of TEM sample. In order to qualitatively evaluate the distribution of Ti in Mg particles, EDS elemental maps of Mg and Ti are shown in Figure 2c and 2d. As can be seen, Ti is homogeneously distributed on the surface or inside Mg particles. The actual Ti weight content in the prepared Mg-Ti nano-composite is determined to be around 1.0 wt% by EDS. The actual Ti content in the Mg-Ti nano-composite is much lower than that in precursors, which is likely due to the fact that the co-precipitated Ti particles are too small to be separated from solution. Only a small amount of Ti particles that are embedded in or attached on the surface of Mg particles can be separated with Mg after the centrifugation and repeated washing processes. The TEM micrograph and the corresponding SAED pattern of the Mg-Ti nano-composite hydrogenated at 75 ^{o}C for 2 h are shown in Figure 3a and 3b, respectively. The diffraction rings or points correspond to Mg, MgO, β-MgH_2 and γ-TiH_2 phases. Only a few diffraction points

can be indexed with the β-MgH_2 phase. This is due to hydrogen release from the nano-sized MgH_2 during the TEM measurement under high-vacuum condition and exposure to the electron beam.[44] As can be seen, the hydrogenated Mg-Ti nano-composite is composed of irregular shaped particles aggregating together with their particle sizes ranging from 20 to 30 nm. The particle size of the hydrogenated Mg-Ti nano-composite is much lower than that of the Mg-Ti nano-composite. The main reasons are as follows. The high density of defects on the Mg particles and at the interfaces between Mg and Ti can serve as nucleation sites for MgH_2 during the hydrogenation process. In addition, the crystallite size of β-MgH_2 will not grow up at such a low absorption temperature (75 ^oC), resulting in a smaller crystallite size of β-MgH_2. In order to reveal the morphology of TiH_2 nanoparticles, a dark field image taken from the diffraction points of γ-TiH_2 (110) and MgO (200) is shown in Figure 3c. It is observed that TiH_2 and MgO nanoparticles with bright contrasts and particle size of several nano-meters are distributed homogeneously on the surface of those large MgH_2 particles.

3.2 Hydrogen sorption properties of the Mg-Ti nano-composite

The PCT curves of the Mg-Ti nano-composite measured at 250, 275, 300, 325, 350, and 375 ^oC in a hydrogen pressure range from 0.02 to 4 MPa are shown in Figure 4a. It is observed that single flat plateaus owing to the formation and decomposition of the MgH_2 phase are present across the whole range of the hydrogen content at each temperature. The maximum hydrogen absorption capacity of the Mg-Ti nano-composite is about 6.8 wt% at 375 ^oC, with fairly close amount of reversible

hydrogen sorption capacity. The Mg-Ti nano-composite can absorb and release hydrogen at temperatures down to 275 ^{o}C. The corresponding van't Hoff plot (ln$P$ versus 1/T) is used to estimate hydrogenation and dehydrogenation enthalpies and entropies, as shown in Figure 4b. The hydrogenation enthalpy ($\triangle H_{ab}$) and entropy ($\triangle S_{ab}$) are determined to be -73.0±1.8 kJ/mol H_2 and 131.9±3.0 J/(mol·K) H_2 while the dehydrogenation enthalpy ($\triangle H_{de}$) and entropy ($\triangle S_{de}$) are 75.8±4.7 kJ/mol H_2 and 134.8±7.9 J/(mol·K) H_2, respectively. The values of enthalpies for the Mg-Ti nano-composite are quite close to those of the standard values for Mg (-74.1± 2.9 kJ/mol H_2),[45] a nanostructured MgH_2/0.1TiH_2 composite prepared by ball milling under high hydrogen pressure ($\triangle H_{de}$=77.4 kJ/mol H_2),[46] and nano-structured Ti-catalyzed MgH_2 prepared by a homogeneously catalyzed synthesis method ($\triangle H_{de}$=77.7 kJ/mol H_2).[30] However, Lu et al. reported a significant reduction of the dehydrogenation enthalpy (68.2 kJ/mol H_2) in a study of a Mg-0.1TiH_2 with a crystallite size of 5~10 nm, prepared by ultrahigh-energy-high-pressure (UHEHP) ball milling. A possible different reaction mechanism of hydrogen with magnesium is attributed to the effects from nano-sized MgH_2 and the addition of TiH_2.[28] In this work, the average crystallite size of Mg-Ti nano-composite is a little larger than that of the Mg-0.1TiH_2. The actual Ti weight content in the Mg-Ti nano-composite is much lower than that of the Mg-0.1TiH_2. In addition, the tetragonal structure of γ-TiH_2 phase is different from the cubic structure of δ-TiH_2, possibly leading to a different catalytic mechanism for hydrogen sorption in Mg. The values of entropies are close to the classical value of 130.6 J/(mol·K) H_2 reported by Stampfer et al..[47]

Considering the above, it is thus reasonable that the addition of Ti in the Mg-Ti nano-composite does not change the hydrogenation and dehydrogenation enthalpies and entropies of Mg.

Figure 5a presents the isothermal hydrogen absorption curves of the Mg-Ti nano-composite measured at different temperatures under 3 MPa hydrogen pressure. The data obtained from hydrogen absorption kinetics measurement is summarized in Table 1. It is observed that the as-prepared sample exhibits excellent hydrogen absorption kinetic properties: the hydrogen capacities can reach up to 6.2, 6.5, and 6.6 wt% in 2 h at 25, 50, and 75 ^{o}C, respectively. 90% of the maximum hydrogen capacity for the Mg-Ti nano-composite can be obtained within 3559, 1665, and 499 s at 25, 50, and 75 ^{o}C, respectively. As can be seen in the inset of Figure 5a, the hydrogenation capacity of the Mg-Ti nano-composite reaches its maximum amount within 2 h at room temperature. In comparison, for Mg nanocrystals prepared by Norberg et al, a hydrogen capacity of nearly 5 wt% can be achieved within 1 h at 220 ^{o}C.[11] Mg-0.1TiH_2 prepared through UHEHP can uptake nearly 4 wt% of hydrogen within 4 h at room temperature.[15] MgH_2/TiH_2 composite prepared through ball milling under high hydrogen pressure can only absorb 1.2 wt% of hydrogen after 5 h and 2 wt% of hydrogen after 20 h at 40 ^{o}C.[46] Above results suggest that Ti added in the co-precipitated Mg-Ti nano-composite has drastic effects on accelerating the hydrogenation rate of Mg. The improved hydrogen absorption kinetics at low temperatures can be further investigated by calculating the activation energy (E_a) of the hydrogenation reaction. The hydrogen absorption data can be analyzed by

applying the Johnson-Mehl-Avrami-Kolmogorov (JMAK) model, which is one of the most effective ways to describe the nucleation and growth model,[48-50] and the linear equation is described as follows:

$$\ln[-\ln(1-\alpha)]=\eta\ln k+\eta\ln t \qquad (3),$$

where α is the fraction of Mg transformed into MgH_2 at time t, k an effective kinetics parameter and η is the Avrami exponent or reaction order. For the absorption at 25, 50 and 75 ^{o}C, by plotting $\ln[-\ln(1-\alpha)]$ vs. $\ln t$, the values of k and η at different temperatures can be obtained by calculting the values of η (the slope) and the $\eta\ln k$ (intercept) of that straight line at each temperature. The apparent activation energy (E_a) for the absorption is usually evaluated according to Arrhenius equation :[48]

$$k=A\bullet\mathrm{Exp}(-E_a/RT) \qquad (4),$$

where A is a temperature independent coefficient, R the universal gas constant, and T is the absolute temperature. The Arrhenius type plot of $\ln k$ vs. $1000/T$ is drawn in Figure 5b. Thus, E_a of the Mg-Ti nano-composite can be determined to be 50.2 kJ/mol H_2, which is much lower than that of Mg Nanocrystals with particle size of 25 nm (122 kJ/mol H_2).[11] Though, E_a of the Mg-Ti nano-composite is larger than that of the MgH_2-0.1TiH_2 reported by Lu et al. (16.4 kJ/mol H_2).[15] The Mg-Ti nano-composite has shown faster hydogen absoption rate than that of the MgH_2-0.1TiH_2. The similar phenomenon was also observed in the Mg-TM-La (TM=transition metal) composite powders[51] and the comparison study between Mg-Y_2O_3 and Mg-Y composites[52], which is a result of the different values of A in different hydrogen storage systems.

It is known that the hydrogenation process of Mg involves the following steps: physisorption of hydrogen molecules, dissociation of H_2 into hydrogen atoms, surface chemisorption of hydrogen atoms, diffusion of hydrogen atoms into bulk, nucleation and growth of the hydride phase.[53] In general, the reduction of particle or crystallite size is an effective method to improve the hydrogen absorption kinetics of Mg, duo to the larger active surface area and shorter diffusion length for hydrogen atoms.[54] However, the nanosize effect alone cannot explain the quite large amount of hydrogen capacity of the Mg-Ti nano-composite obtained at room temperature as obseved in this work. The co-precipiated Ti is thus responsible for the drastic improvement in the hydrogen absorption kinetics. The energy of hydrogen dissociation on a pure Mg(0001) surfare is ~1.15ev,[55] while for the Ti-incorporated Mg(0001) surface, the activated barrier decreases to 0.103 eV due to the strong interaction between the molecular orbital of hydrogen and the *d* shell of Ti.[56] Also, Ti can help to split hydrogen molecule into atoms ready for diffusion into the bulk. Moreover, duo to the modified electronic configuration, the H atoms dissociated on Ti can detach from Ti and then spill over into the Mg matrix.[57] Wang et al. have pointed out that the catalytic effectiveness depends not only on the intrinsic activity of the catalyst, but also on its distribution state.[58] In this work, Ti and Mg particles were co-precipitated from the solution to obtain the Mg-Ti nano-composite with homogeneous distribution of Ti in Mg particles. The interaction between Ti and Mg can be enhanced by such a special distribution state, resulting in an improvement of the absorption kinetics.

Further more, as mentioned above, γ-TiH_2 can be formed during the absoption

process. Cuevas et al. have found that TiH_2 phase formed during the early stage of absorption, while MgH_2 phase is obseved during the later stage, for Mg-Ti powder mixtures prepared by reactive ball milling under hydrogen gas.[27] Griessen et al. have reported that the standard enthalpy of TiH_2 is -149.24 kJ/mol H_2,[59] which is much lower than that of MgH_2 (-74.1± 2.9 kJ/mol H_2).[45] These results suggest that TiH_2 may form before the formation of MgH_2 during the initial absoption process of the Mg-Ti nano-composite. It is well known that TiH_2 is a good catalyst for improving the absorption kinetics of Mg.[15, 28, 46] The interfaces between TiH_2 and Mg matrix can act as active sites to provide the nucleation and growth centers for the MgH_2 phase. In our work, the tetragonal γ-TiH_2 is not the same as what is observed in other Mg-Ti-H systems, which likely results in a better catalytic effect on the absorption kinetics of Mg. Therefore, the co-operation between Ti and the tetragonal γ-TiH_2 formed later leads to a high catalytic efficiency on enhancing the absorption kinetics performance of Mg.

DSC curves and the corresponding $\ln(\beta/T_p^2)$-$1000/T_p$ plots for the hydrogenated Mg-Ti nano-composite are shown in Figure 6. As can be seen in Figure 6a, a broad endothermic peak corresponding to the desorption of β-MgH_2 and γ-MgH_2 phases appears upon heating of the hydrogenated Mg-Ti nano-composite. The peak desorption temperatures of the hydrogenated Mg-Ti nano-composite at heating rates of 3, 5 and 10 ^oC/min are 317.5, 326.9 and 340.0 ^oC, respectively. The onset dehydrogenation temperature at a heating rate of 3 ^oC/min is 296.1^oC. In contrast, it is about 340 ^oC for the MgH_2 without catalysts after 100 h of ball milling.[60] The

desorption activation energy, E_d, of the Mg-Ti nano-composite can be estimated by using the Kissinger equation:[61]

$$\ln(\beta/T_p^2)=\text{A}-E_d/(\text{R}T_p) \qquad (5),$$

where β is the heating rate, T_p the peak temperature, and A is a linear constant. The E_d value for the Mg-Ti nano-composite is determined to be 170.9 kJ/mol H_2 based on the plot of $\ln(\beta/T_p^2)$ vs.$1000/T_p$, as shown in Figure 6b. This value is lower than 250 kJ/mol H_2 reported for the ball milled pure MgH_2 and 208 kJ/mol H_2 reported for the Mg-1at%Ti.[62] The improved hydrogen desorption kinetics and lower E_d value indicate that the γ-TiH_2 formed during the absorption process has high catalytic efficiency in enhancing the desorption kinetics of nanosized Mg.

4. Conclusions

In this work, a Mg-Ti nano-composite was successfully co-precipitated from a homogeneous THF solution including anhydrous $MgCl_2$, $TiCl_4$ and LiNp as the reducing agent. The microsturcture features and hydrogen sorption properties of the Mg-Ti nano-composite were carefully investigated. The main conclusions are as follows:

(1) TEM and STEM observations revealed that the Mg-Ti nano-composite contained nearly 1.0 wt% of Ti distributed homogenously on the surface or inside those Mg nano-particles.

(2) γ-MgH_2 and the tetragonal γ-TiH_2 were obtained when the Mg-Ti nano-composite was hydrogenated at 75 ^{o}C.

(3) The Mg-Ti nano-composite showed superior hydrogen absorption properties.

For instance, its maximum hydrogen capacity can reach up to 6.2 wt% within 2 h at room temperature under a hydrogen pressure of 3 MPa. The improved hydrogen absorption kinetics at low temperatures was in consistent with the low activation energy for hydrogen absorption (50.2 kJ/mol H_2).

(4) Based on the PCT measurements, the hydrogenation and dehydrogenation enthalpies of the nano-composite were calculated to be-73.0±1.8 and 75.8±4.7 kJ/mol H_2, close to the standard values for Mg (-74.1± 2.9 kJ/mol H_2).

(5) The co-precipitated Ti and the tetragonal γ-TiH_2 formed during hydrogenation process have a high catalytic efficiency in enhancing the asorption kinetics of the nanosized Mg without changing the hydrogen sorption themodynamics.

Acknowledgment

Prof. Zou would like to thank the support from the Science and Technology Committee of Shanghai under No. 10JC1407700, No. 11ZR1417600, and 'Pujiang' project (No. 11PJ1406000). This work is partly supported by the Research Fund for the Doctoral Program of Higher Education of China (No. 20100073120007) and from the Shanghai education commission (No. 12ZZ017).

Notes and References

1. R. Bardhan, A. M. Ruminski, A. Brand and J. J. Urban, *Energy Environ. Sci.,*2011, **4**, 4882-4895.
2. F. Cheng, Z. Tao, J. Liang and J. Chen, *Chem. Commun.*, 2012, **48**, 7334-7343.
3. G. Liang, *J. Alloys Compd.*, 2004, **370**, 123-128.
4. A. Zaluska, L. Zaluski and J. Ström-Olsen, *Appl. Phys. A,* 2001, **72**, 157-165.
5. N. Hanada, T. Ichikawa and H. Fujii, *J. Phy. Chem. B*, 2005, **109**, 7188-7194.
6. I. Malka, T. Czujko and J. Bystrzycki, *Int. J. Hydrogen Energy*, 2010, **35**, 1706-1712.
7. W. Oelerich, T. Klassen and R. Bormann, *J. Alloys Compd.*, 2001, **315**, 237-242.
8. J. Huot, G. Liang, S. Boily, A. Van Neste and R. Schulz, *J. Alloys Compd.*, 1999, **293**, 495-500.
9. K.-J. Jeon, H. R. Moon, A. M. Ruminski, B. Jiang, C. Kisielowski, R. Bardhan and J. J. Urban,

Nat. Mater., 2011, **10**, 286-290.

10. Z. Zhao-Karger, J. Hu, A. Roth, D. Wang, C. Kübel, W. Lohstroh and M. Fichtner, *Chem. Commun.*, 2010, **46**, 8353-8355.
11. N. S. Norberg, T. S. Arthur, S. J. Fredrick and A. L. Prieto, *J. Am. Chem. Soc.*, 2011, **133**, 10679-10681.
12. J. Pelletier, J. Huot, M. Sutton, R. Schulz, A. Sandy, L. Lurio and S. Mochrie, *Phy. Rev. B*, 2001, **63**, 052103.
13. X. Tan, B. Zahiri, C. M. B. Holt, A. Kubis and D. Mitlin, *Acta Mater.*, 2012, **60**, 5646-5661.
14. J. Lu, Y. J. Choi, Z. Z. Fang, H. Y. Sohn and E. Rönnebro, *J. Am. Chem. Soc.*, 2010, **132**, 6616-6617.
15. T. Ma, S. Isobe, Y. Wang, N. Hashimoto and S. Ohnuki, *J. Phy. Chem. C.*, 2013.
16. E. Grigorova, M. Khristov, P. Peshev, D. Nihtianova, N. Velichkova and G. Atanasova, *Bulg. Chem. Commun.*, 2013, **45**, 280-287.
17. S. K. Pandey, A. Bhatnagar, R. R. Shahi, M. Hudson, M. K. Singh and O. Srivastava, *J. Nanosci. Nanotechno.*, 2013, **13**, 5493-5499.
18. L. P. Ma, X. D. Kang, H. B. Dai, Y. Liang, Z. Z. Fang, P. J. Wang, P. Wang and H. M. Cheng, *Acta Mater.*, 2009, **57**, 2250-2258.
19. L. Xie, Y. Liu, Y. T. Wang, J. Zheng and X. G. Li, *Acta Mater.*, 2007, **55**, 4585-4591.
20. S. Jin, J. Shim, J. Ahn, Y. Cho and K. Yi, *Acta Mater.*, 2007, **55**, 5073-5079.
21. H. Imamura and N. Sakasai, *J. Alloys Compd.*, 1995, **231**, 810-814 .
22. H. Imamura, N. Sakasai and Y. Kajii, *J. Alloys Compd.*, 1996, **232**, 218-223.
23. H. Imamura, N. Sakasai and T. Fujinaga, J. Alloys Compd., 1997, **253 -254**, 34-37.
24. C. Milanese, A. Girella, G. Bruni, V. Berbenni, P. Cofrancesco, A. Marini, M. Villa and P. Matteazzi, *J. Alloys Compd.*, 2008, **465**, 396-405.
25. T. K. Nielsen, F. Besenbacher and T. R. Jensen, *Nanoscale*, 2011, **3**, 2086-2098.
26. G. Liang, J. Huot, S. Boily, A. Van Neste and R. Schulz, *J. Alloys Compd.*, 1999, **292**, 247-252.
27. F. Cuevas, D. Korablov and M. Latroche, *Phys. Chem. Chem. Phys.*, 2012, **14**, 1200-1211.
28. J. Lu, Y. J. Choi, Z. Z. Fang, H. Y. Sohn and E. Rönnebro, *J. Am. Chem. Soc.*, 2009, **131**, 15843-15852.
29. C. Zhou, Z. Z. Fang, C. Ren, J. Li and J. Lu, *J. Phy. Chem. C.*, 2013, **117**, 12973-12980.
30. H. Shao, M. Felderhoff, F. Schüth and C. Weidenthaler, *Nanotechnology*, 2011, **22**, 235401.
31. J. Cui, H. Wang, J. Liu, L. Ouyang, Q. Zhang, D. Sun, X. Yao and M. Zhu, *J. Mater. Chem. A*, 2013, 1, 5603
32. M. Ephritikhine, *Chem. Commun.*, 1998, 2549-2554.
33. T. Tsuritani, S. Ito, H. Shinokubo and K. Oshima, *J. Org. Chem.*, 2000, **65**, 5066-5068.
34. K. Wang, S. X. Wang, M. Z. Gao and J. T. Li, *S Synth. Commun.*, 2006, **36**, 1391-1399.
35. R. D. Rieke and S. E. Bales, *J. Am. Chem. Soc.*, 1974, **96**, 1775-1781.
36. L. S. Birks, H. Friedman, *J. Appl. Phy.*, 1946, **17**, 687-692.
37. G. Siviero, V. Bello, G. Mattei, P. Mazzoldi, G. Battaglin, N. Bazzanella, R. Checchetto and A. Miotello, *Int. J. Hydrogen Energy*, 2009, **34**, 4817-4826.
38. Y. K. Gautam, A. K. Chawla, R. Walia, R. Agrawal and R. Chandra, *Appl. Surf. Sci.*, 2011, **257**, 6291-6295.
39. E. Lunarska, O. Chernyayeva, D. Lisovytskiy and R. Zachariasz, *Mate.r Sci. Eng. C*, 2010, **30**,

181-189.
40. E. Łunarska, O. Chernyayeva and D. Lisovytskiy, *Adv. Mater. Sci.*, 2008, **8**, 105-114.
41. E. Lunarska, O. Chernyaeva and D. Lisovytskii, *Mater. Sci.,* 2008, **44**, 423-428.
42. H.-C. Cheng, S.-Y. Lee, C.-C. Chen, Y.-C. Shynge and K.-L. Ou, *J. Electrochem. Soc.*, 2007, **154**, E13-E18.
43. C.E. Nelson, *Trans. AFS*, 1948, **56**, 1–23.
44. N. Hanada, E. Hirotoshi, T. Ichikawa, E. Akiba and H. Fujii, *J. Alloys Compd.*, 2008, **450**, 395-399.
45. J.A. Kennelley, J.W. Varwig, H.W. Myers, *J. Am. Chem. Soc.*,1960, **64**, 703-704.
46. H. Shao, M. Felderhoff, F. Schüth, *Int. J. Hydrogen Energy*, 2011, **36**, 10828-10833.
47. J. F. Stampfer Jr, C. E. Holley Jr, J. F. Suttle, *J. Am. Chem. Soc.*, 1960, **82**, 3504-3508.
48. N. Bazzanella, R. Checchetto and A. Miotello, *Appl. Phys. Lett.*, 2004, **85**, 5212-5214.
49. K. F. Kelton, *Mater. Sci. Eng. A*, 1997, **226**, 142-150.
50. M. H. Mintz and Y. Zeiri, *J. Alloys Compd.*, 1995, **216**, 159-175.
51. J. Zou, H. Guo, X. Zeng, S. Zhou, X. Chen and W. Ding, *Int. J. Hydrogen Energy*, 2013, **38**, 8852-8862.
52. S. Long, J. Zou, X. Chen, X. Zeng and W. Ding, *J. Alloys Compd.*, 2013.
53. H. G. Schimmel, J. Huot, L. C. Chapon, F. D. Tichelaar and F. M. Mulder, *J. Am. Chem. Soc.*, 2005, **127**, 14348-14354.
54. A. Zaluska, L. Zaluski, Ström-Olsen JO, *J. Alloy Compd.*, 1998, **288**, 217-225.
55. T. Vegge, *Phy. Rev. B*, 2004, **70**, 035412.
56. A. Du, S. C. Smith, X. Yao and G. Lu, *J. Phy. Chem. B*, 2005, **109**, 18037-18041.
57. L.-P. Ma, X.-D. Kang, H.-B. Dai, Y. Liang, Z.-Z. Fang, P.-J. Wang, P. Wang and H.-M. Cheng, *Acta Mater.*, **2009**, 57, 2250-2258.
58. P. Wang, X.-D. Kang and H.-M. Cheng, *J. Phy. Chem. B*, 2005, **109**, 20131-20136.
59. R. Griessen and T. Riesterer, in *Hydrogen in intermetallic compounds I*, Springer, 1988, pp. 219-284.
60. R. A. Varin, T. Czujko, Z. Wronski, *Nanotechnology*, 2006, **17**, 3856
61. H. E. Kissinger, *Anal. Chem.*, 1957, **29**, 1702.
62. H. B. Lu, C. K. Poh, L. C. Zhang, Z. P. Guo, X. B. Yu, H. K. Liu, *J. Alloys Compd.*, **481**, 152-155.

Figure captions

Figure 1. XRD patterns of the Mg-Ti nano-composite in varying states. (a) as prepared, (b) hydrogenated at 75 ^{o}C for 2 h, and (c) rehydrogenated at 75 ^{o}C after dehydrogenation at 300 ^{o}C. Inset shows XRD patterns of b and c in the 2Theta range of 25~45°.

Figure 2. (a) STEM micrograph and (b) SAED pattern of the Mg-Ti nano-composite, and along with (c, d) EDS elemental maps of Mg and Ti.

Figure 3. (a) TEM micrograph and (b) SAED pattern of the Mg-Ti nano-composite hydrogenated at 75 ^{o}C, and (c) the corresponding dark field TEM image of γ-TiH_2/MgO nanoparticles.

Figure 4. (a) PCT curves of the Mg-Ti nano-composite measured at different temperatures and (b) the corresponding van't Hoff plots. Ab-absorption, De-desorption.

Figure 5. (a) Hydrogen absorption curves of the Mg-Ti nano-composite measured at different temperatures for 2 h, and (b) the corresponding ln$k$-1000/T plot. Inset of (a) shows the hydrogen absorption curve measured at 25 ^{o}C for 10 h.

Figure 6. DSC curves (a) and the corresponding $\ln(\beta/T_p^2)$-$1000/T_p$ plots (b) for the hydrogenated Mg-Ti nano-composite.

Table captions

Table 1. Hydrogen absorption data for the Mg-Ti nano-composite obtained at different temperatures

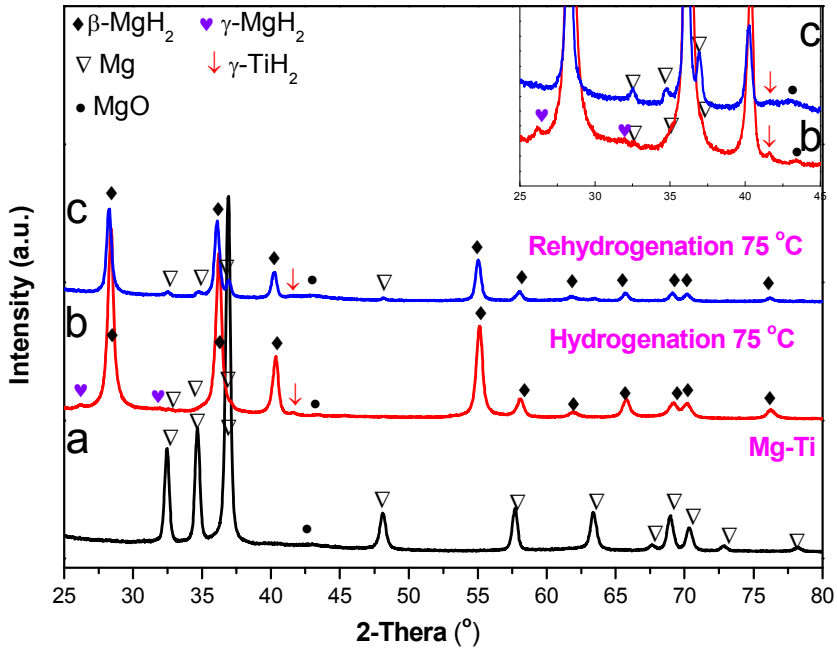

Figure 1. XRD patterns of the Mg-Ti nano-composite in varying states. (a) as prepared, (b) hydrogenated at 75 ^{o}C for 2 h, and (c) rehydrogenated at 75 ^{o}C after dehydrogenation at 300 ^{o}C. Inset shows XRD patterns of b and c in the 2Theta range of 25~45°.

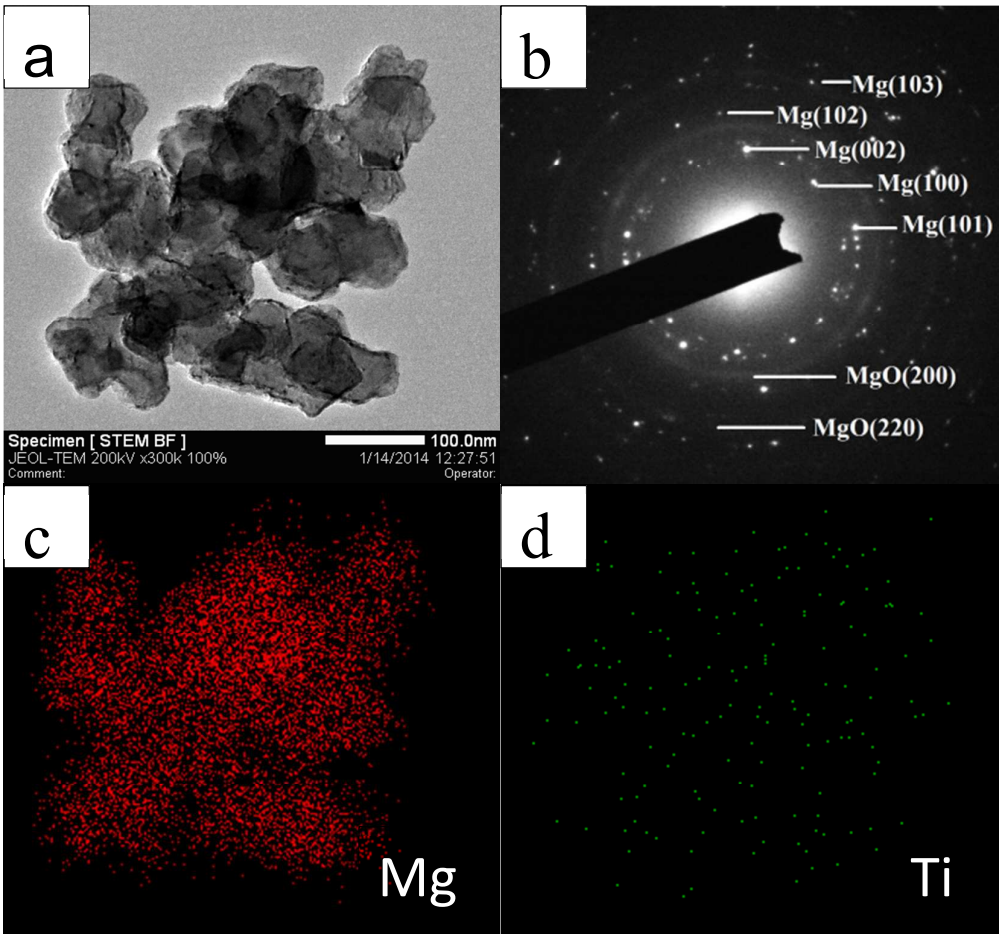

Figure 2. (a) STEM micrograph and (b) SAED pattern of the Mg-Ti nano-composite, and along with (c, d) EDS elemental maps of Mg and Ti.

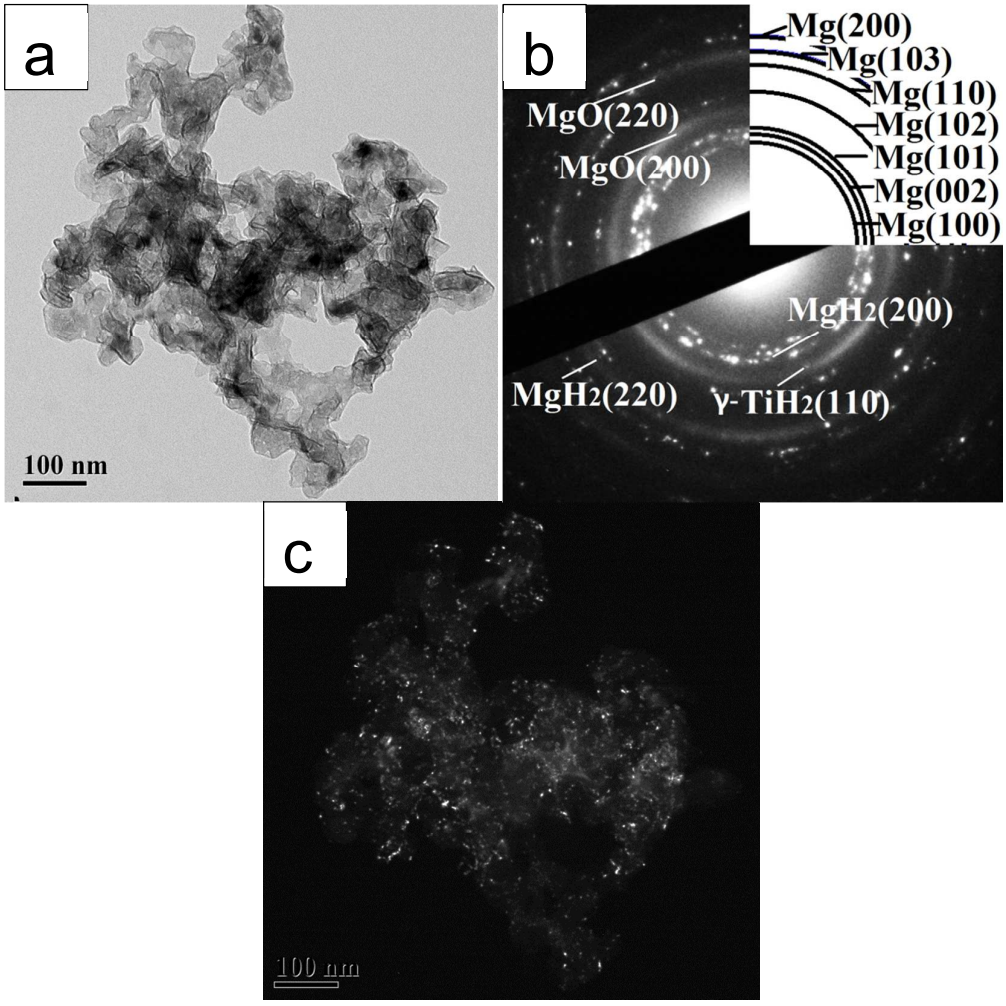

Figure 3. (a) TEM micrograph and (b) SAED pattern of the Mg-Ti nano-composite hydrogenated at 75 ^{o}C, and (c) the corresponding dark field TEM image of γ-TiH_2/MgO nanoparticles.

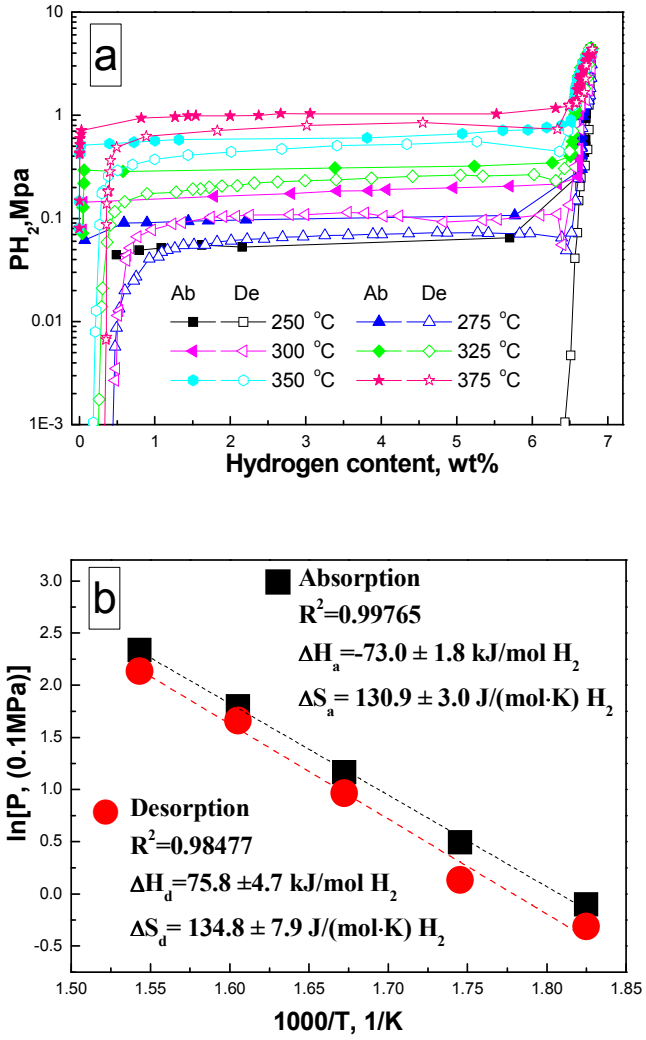

Figure 4. (a) PCT curves of the Mg-Ti nano-composite measured at different temperatures and (b) the corresponding van't Hoff plots. Ab-absorption, De-desorption.

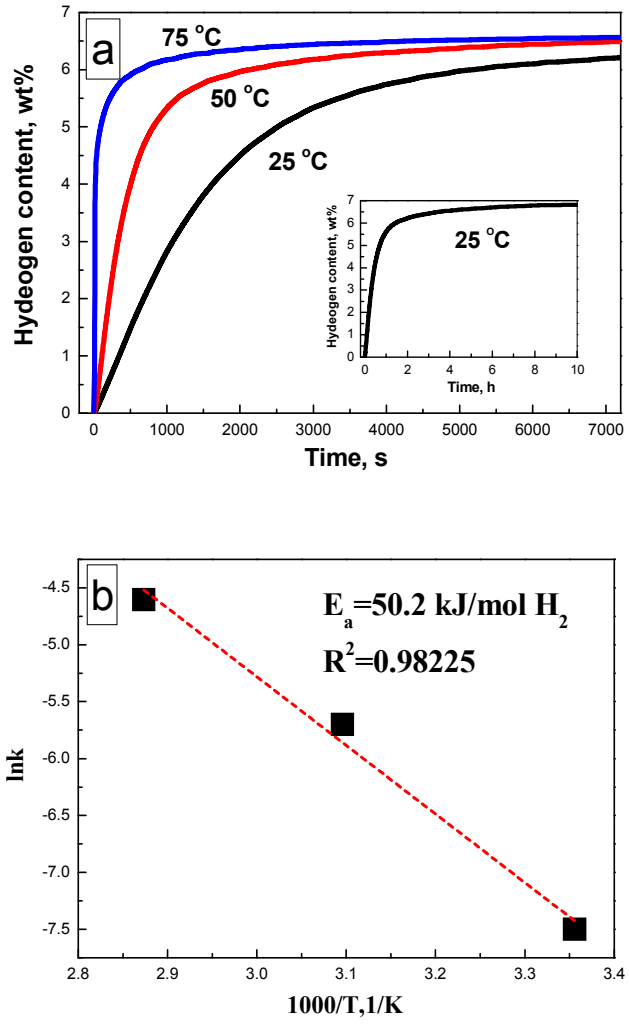

Figure 5. (a) Hydrogen absorption curves of the Mg-Ti nano-composite measured at different temperatures for 2 h, and (b) the corresponding ln*k*-1000/*T* plot. Inset of (a) shows the hydrogen absorption curve measured at 25 °C for 10 h.

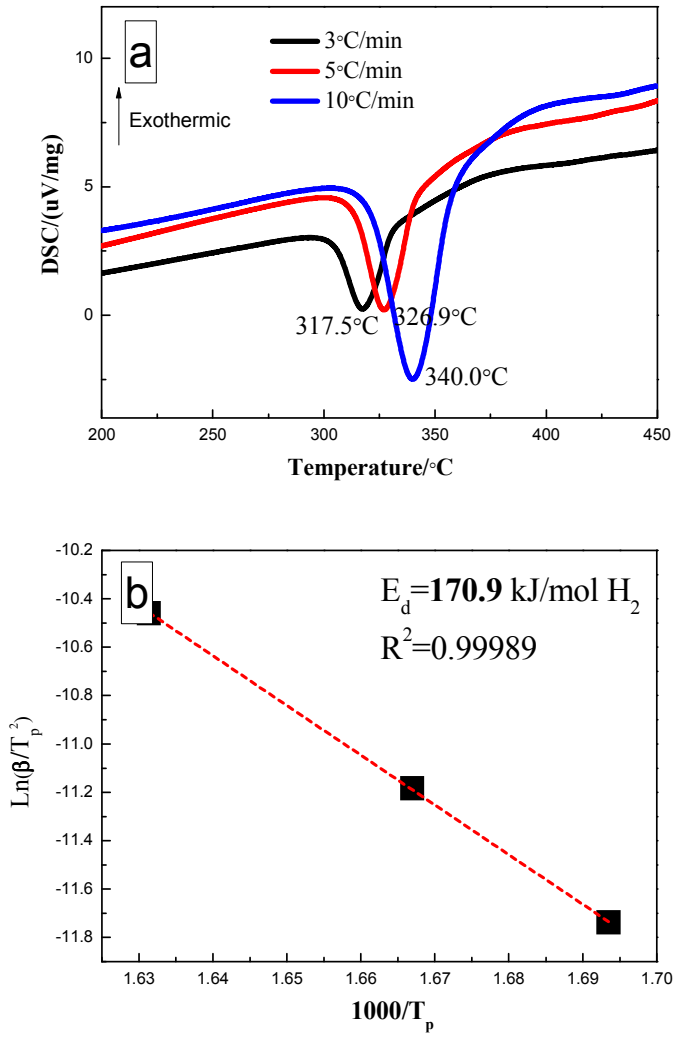

Figure 6. (a) DSC curves and (b) the corresponding $\ln(\beta/T_p^2)$-$1000/T_p$ plots for the hydrogenated Mg-Ti nano-composite.

Table 1. Hydrogen absorption data for the Mg-Ti nano-composite obtained at different temperatures

Temperature (^{o}C)	Cmax-hydrogen capacity after 2 h (wt %)	Time needed to 90 % Cmax (s)	Time needed to 80 % Cmax (s)	Time needed to 70 % Cmax (s)
75	6.6	499	144	46
50	6.5	1665	915	639
25	6.2	3559	2478	1873